TOXICOLOGICAL SCIENCES **120(1)**, 123–135 (2011)
doi:10.1093/toxsci/kfq363
Advance Access publication December 6, 2010

Comparative Proteomics and Pulmonary Toxicity of Instilled Single-Walled Carbon Nanotubes, Crocidolite Asbestos, and Ultrafine Carbon Black in Mice

Justin G. Teeguarden,*[,1] Bobbie-Jo Webb-Robertson,* Katrina M. Waters,* Ashley R. Murray,† Elena R. Kisin,† Susan M. Varnum,* Jon M. Jacobs,* Joel G. Pounds,* Richard C. Zanger,* and Anna A. Shvedova†

*Pacific Northwest National Laboratory, Richland, Washington 99352; and †National Institute of Occupational Health and Safety, Morgantown, West Virginia 26505-2888

[1]To whom correspondence should be addressed at Pacific Northwest National Laboratory, 902 Battelle Boulevard, Richland, WA 99352. Fax: (509) 371-6978. E-mail: justin.teeguarden@pnl.gov.

Received August 3, 2010; accepted November 30, 2010

Reflecting their exceptional potential to advance a range of biomedical, aeronautic, and other industrial products, carbon nanotube (CNT) production and the potential for human exposure to aerosolized CNTs are increasing. CNTs have toxicologically significant structural and chemical similarities to asbestos (AB) and have repeatedly been shown to cause pulmonary inflammation, granuloma formation, and fibrosis after inhalation/instillation/aspiration exposure in rodents, a pattern of effects similar to those observed following exposure to AB. To determine the degree to which responses to single-walled CNTs (SWCNT) and AB are similar or different, the pulmonary response of C57BL/6 mice to repeated exposures to SWCNTs, crocidolite AB, and ultrafine carbon black (UFCB) were compared using high-throughput global high performance liquid chromatography fourier transform ion cyclotron resonance mass spectrometry (HPLC-FTICR-MS) proteomics, histopathology, and bronchoalveolar lavage cytokine analyses. Mice were exposed to material suspensions (40 micrograms per mouse) twice a week for 3 weeks by pharyngeal aspiration. Histologically, the incidence and severity of inflammatory and fibrotic responses were greatest in mice treated with SWCNTs. SWCNT treatment affected the greatest changes in abundance of identified lung tissue proteins. The trend in number of proteins affected (SWCNT [376] > AB [231] > UFCB [184]) followed the potency of these materials in three biochemical assays of inflammation (cytokines). SWCNT treatment uniquely affected the abundance of 109 proteins, but these proteins largely represent cellular processes affected by AB treatment as well, further evidence of broad similarity in the tissue-level response to AB and SWCNTs. Two high-sensitivity markers of inflammation, one (S100a9) observed in humans exposed to AB, were found and may be promising biomarkers of human response to SWCNT exposure.

Key Words: **nanomaterials; risk assessment; proteomics; asbestos; SWCNT.**

Disclaimer: The findings and conclusions in this report are those of the authors and do not necessarily represent the views of the National Institute for Occupational Safety and Health.

Discovered more than 20 years ago (Ijima, 1991), carbon nanotubes (CNT) are nonetheless a toxicologically new class of carbon/graphitic materials that include single-walled (SW) and multiwalled (MW) materials in various forms of purity, particularly with respect to metals and metal oxide residues from their manufacture, sizes, and modifications to their surface chemistry. The potential for their unique conductive and electrochemical properties (Baughman *et al.*, 2002) to revolutionize a wide spectrum of products continues to drive exponential growth in research (Baughman *et al.*, 2002) and commercial production (Thayer, 2007). CNTs have emerged as a nanomaterial of considerable concern to the occupational and environmental health and safety communities because of their high production and use rates, measured, but low human workplace exposure (Maynard *et al.*, 2004), and early, consistent reports from high-dose, short-term screening studies in rodents that suggest a sequence of biological events and pulmonary pathology similar to that caused by asbestos (AB) and synthetic vitreous fibers (SVF) (Donaldson *et al.*, 2008).

With a notable exception of the study by Shvedova *et al.* (2008b), the high cost and difficulty of engineering well-characterized, controlled exposures to aerosolized CNTs have limited the conduct of chronic rodent inhalation studies of CNTs. Multiple, single-dose, exploratory, or mechanistic studies of the pulmonary toxicity of both MWCNTs and SWCNTs utilizing either the pharyngeal aspiration (p.a., mouse only) or the intratracheal instillation methods of delivery have been conducted. Despite some limitations of a nonphysiological method of delivery to target tissue and in some cases high doses suitable for hazard screening, these studies provide important information about the potential for CNTs to damage pulmonary tissues. The studies are consistent and collectively support a common sequence of biological events following single CNT exposure: robust acute-phase inflammation

consistent with a foreign body response, followed by formation of multifocal granulomas, and in most cases an early onset fibrosis (Table 1) (Chou *et al*., 2008; Lam *et al*., 2004; Muller *et al*., 2005; Shvedova *et al*., 2007, 2008a, 2008b; Warheit *et al*., 2004). The acute-phase inflammation is characterized by polymorphonuclear leukocytes (PMN) and macrophage influx and release of proinflammatory cytokines including tumor necrosis factor alpha (TNF-α), interleukin (IL) 6, IL-1β, and monocyte chemotactic protein 1 (Muller *et al*., 2005; Shvedova *et al*., 2005, 2008c). Granulomas form around CNT agglomerates but also appear distal to the agglomerates where dispersed CNTs are believed to be present (Shvedova *et al*., 2005). Fibrosis occurs both within granulomas and as diffuse interstitial and septal fibrosis distal to granulomas (Muller *et al*., 2008; Shvedova *et al*., 2005).

CNTs and AB share structural and chemical features that are, in the case of AB, related to the potential to cause pulmonary toxicity, fibrogenesis, and cancer. These features include size and shape, particularly a long aspect ratio, biopersistence, and presence of transition metals and/or the ability to generate reactive oxygen species (Pacurari *et al*., 2010; Sanchez *et al*., 2009).

The key biological and toxicological events in the lung following single pulmonary exposures to CNTs in rodents are consistent with those of AB-induced pulmonary damage: inflammation followed by pulmonary fibrosis (Pacurari *et al*., 2010). Although it is tempting to accept this observation as sufficient evidence for a common mode of action between these materials and the implication of high risk of human disease from CNT exposure, it must be noted that all the studies focused on pulmonary inflammation and related endpoints, and no broad, comprehensive studies of pulmonary responses to CNTs and AB in these models have been conducted. Donaldson was careful to point out that it was not yet clear if CNTs followed the AB/SVF fiber toxicology paradigm and that "... other paradigms, as yet unknown, could be involved in the pathogenicity of other fiber types such as CNTs (Donaldson *et al*., 2008)." It is also plausible, as Pauluhn, (2010) has hypothesized, that CNT toxicity following inhalation is related to the well-known phenomena of particle overload.

The objectives of our study were to assess broadly and compare the pulmonary response to repeated exposure to SWCNT, crocidolite AB, and ultrafine carbon black (UFCB) in the mouse model by applying and integrating both conventional toxicological assays and high-throughput, high-information content, global proteomics, and multiplexed protein microELISA analyses. An additional goal of this integrated research program was to enable the identification of unique protein biosignatures of each of the three test compounds, enabling development of rapid screening tools for application to the toxicological assessment of emerging fiber nanoparticles.

MATERIALS AND METHODS

Animals

Specific pathogen-free adult female C57BL/6 mice (8–10 weeks) were supplied by Jackson Laboratories (Bar Harbor, MN) and weighed 20.0 ± 1.9 g when used. Animals were housed one mouse per cage receiving high efficiency particulate air-filtered air in Association for Assessment and Accreditation of Laboratory Animal Care-approved National Institute of Occupational Health (NIOSH) animal facilities. All animals were acclimated in the animal facility under controlled temperature and humidity for 1 week prior to use. Beta Chips (Northeastern Products Corp., Warrensburg, NY) were used for beddings and changed weekly. Animals were supplied with water and certified chow 5020 (Purina Mills, Richmond, IN) *ad libitum* in accordance with guidelines and policy set forth by the Institute of Laboratory Animals Resources, National Research Council. All experimental procedures were conducted in accordance with a protocol approved by the NIOSH Institutional Animal Care and Use Committee.

TABLE 1
Summary of Rodent CNT Toxicity Studies Showing Consistency in the Pulmonary Response to CNT

Material[a]	Species/route/doses (μg/animal)	Study Duration (days)	Acute inflammation	Granuloma	Fibrosis[b]	Reference
M-MWCNT	Rat/i.t./(2000)	3, 60	Y	Y	Y	Muller *et al*., (2008)
UP-SWCNT	Mice/i.t./(100, 500)	4, 90	Y	Y	NR	Lam *et al*., (2004)
P-SWCNT	Mice/i.t./(100, 500)	4, 90	Y	Y	NR	Lam *et al*., (2004)
P-MWCNT	Rats/i.t./(500–5000)	60	Y	Y	Y	Muller *et al*., (2005)
P-SWCNT	Mice/p.a./(10–40)	1, 3, 7, 28, 60	Y	Y	Y	Shvedova *et al*., (2005)
P-SWCNT	Mice[c]/p.a./(40)	1, 7, 28	Y	Y	Y	Shvedova *et al*., (2008c)
P-SWCNT	Mice/p.a./(40)	1, 7, 28	Y	Y	Y	Shvedova *et al*., (2007)
UP-SWCNT	Mice/i.t./(500)	3, 14	Y	Y	NR	Chou *et al*., (2008)
UP-SWCNT	Rats/i.t./(1000, 5000)	1, 7, 30, 90	Y	Y	NR	Warheit *et al*., (2004)
UP-SWCNT	Mice/p.a./(5, 10, 20)	1, 7, 28	Y	NR	Y	Shvedova *et al*., (2008b)
UP-SWCNT	Mice/i/(5)	1, 7, 28	Y	Y	Y	Shvedova *et al*., (2008b)
P-MWCNT	Rat/i/(4.6.8, 243, 1170)	90	Y	Y	Y	Ma-Hock *et al*., (2009)

Note. NR, Not reported.
[a]P, purified; UP, unpurified; M, multiple forms of CNT; i, inhalation; i.t., intratracheal instillation.
[b]Histopathological or biochemical (hydroxyl proline or collagen levels) evidence.
[c]NADPH oxidase–deficient mice.

Experimental Design

There were four treatment groups, saline controls, UFCB, crocidolite AB, and SWCNTs. Each treatment group was composed of six animals for bronchoalveolar lavage (BAL) analysis, six animals for histopathology, and six animals for proteomics. Suspensions of nanomaterials (40 micrograms per mouse, 50 μl) were used for repeated p.a., whereas the corresponding control mice were administered sterile Ca^{2+} + Mg^{2+} free PBS (50 μl) vehicle. Mice were exposed twice a week (Monday and Thursday) at 9 AM for 3 weeks and a total of six doses. The total dose was 240 micrograms per mouse. Mice were sacrificed 24 h following the last exposure. Inflammation was evaluated by total cell and differential cell counts in BAL fluid (BALF); fibrogenic responses to exposed materials were assessed by collagen deposition.

Materials

SWCNTs (CNI Inc., Houston, TX) used in this study were produced by the high-pressure CO disproportionation process technique and purified by acid treatment to remove metal contaminates as described previously (Shvedova *et al*., 2005). SWCNTs contained elemental carbon (99.7% wt) and Fe (0.23% wt); the diameter of nanotubes in the samples ranged from 0.4 to 1.2 nm; and the specific surface area was 1040 m^2/g. The SWCNTs have a length from 0.5 to 1 to 2 μm (Witasp *et al*., 2009). Unpurified SWCNTs contain much larger amounts of Fe and elicit a more profound oxidative stress and pronounced pulmonary responses (Shvedova *et al*., 2008c). A Union for International Cancer Control sample of standard crocidolite AB (18% Fe) had a mean diameter of 210 nm, surface area 8.3 + 0.5 m^2/g, and length of 0.8–12 μm (Kisin *et al*., 2010). UFCB used in this study had a mean diameter of 14.3 nm and surface area of 253.9 m^2/g. Characterization methods for UFCB and SWCNTs were described previously by Shvedova *et al*. (2005). The surface area doses of SWCNTs and UFCB were 125 or 30 times higher than the surface area dose of AB, respectively.

Dose Selection

Equivalent mass doses of SWCNTs and UFCB (40 micrograms per mouse at each dosing) were used to be consistent with a larger body of literature on the pulmonary effects of these materials (Shvedova *et al*., 2005). The alternative, surface area equivalent doses were not explored because there is no accepted basis for comparing the dose of fibers (AB and SWCNTs) and nonfiber particles (UFCB) because the latter lacks a major determinant of potency, namely, aspect ratio. It was not possible to modulate doses to assure the effective dose to the various regions of the lung for each particle would be similar to that observed following inhalation rather than p.a.; there is insufficient information on the deposition pattern of all three materials by these two routes of administration.

Nanomaterial Aspiration

Repeated p.a. was used for nanomaterial administration (Rao *et al*., 2003). Briefly, after anesthetization with a mixture of ketamine and xylazine (62.5 and 2.5 mg/kg sc in the abdominal area), the mouse was placed on a board in a near vertical position and the animal's tongue extended with lined forceps. A suspension of 40 μg SWCNTs, AB, or UFCB in 50 μl PBS was placed posterior on the throat and the tongue that was held until aspirated into the lungs. Control mice were administered sterile Ca^{2+} + Mg^{2+} free PBS vehicle. The mice revived unassisted after approximately 30–40 min. All mice in SWCNT, AB, UFCB, and PBS groups survived this exposure procedure. This technique provided good distribution of nanomaterials widely disseminated in a peribronchiolar pattern within the alveolar region as was detected by histopathology. Animals treated with the nanomaterials or PBS recovered easily after anesthesia with no behavioral or negative health outcomes. Mice were sacrificed 24 h following the last exposure.

Obtaining BAL from Mice

Mice were weighed and sacrificed with ip injection of sodium pentobarbital (> 100 mg/kg) and exsanguinated. The trachea was cannulated with a blunted 22-gauge needle, and BAL was performed using cold sterile PBS at a volume of 0.9 ml for first lavage (kept separate) and 1.0 ml for subsequent lavages. Approximately 5 ml of BALF per mouse was collected in sterile centrifuge tubes. Pooled cells from each individual mouse BALF were washed in PBS by alternate centrifugation (800 × g, 10 min, 4°C) and resuspension. Cell-free first fraction BAL aliquots were frozen at −80°C until processed.

BAL Cell Counting and Differentials

The degree of inflammatory response induced by the repeated pharyngeally aspirated SWCNTs, AB, or UFCB was estimated by quantitating total cells, macrophages, and PMNs recovered by BAL. Cell counts were performed using an electronic cell counter equipped with a cell-sizing attachment (Coulter model Multisizer II with a 256C channelizer, Coulter Electronics, Hialeah, FL). Alveolar macrophages (AM) and PMNs were identified by their characteristic cell shape in cytospin preparations stained with Diffquick (Fisher Scientific, Pittsburgh, PA), and differential counts of BAL cells were carried out. Three hundred cells per slide were counted.

Lung Preparation for Microscopic Evaluation

Animals were deeply anesthetized with an overdose of sodium pentobarbital by sc injection in the abdomen, the trachea was cannulated, laparotomy performed, and mice sacrificed by exsanguination. The pulmonary artery was cannulated via the ventricle and an outflow cannula inserted into the left atrium. In quick succession, the tracheal cannula was connected to a 5-cm H_2O pressure source, and clearing solution (saline with 100 U/ml heparin, 350 mOsm sucrose) was perfused to clear blood from the lungs. The perfusate was then switched to glutaraldehyde (2%), formaldehyde (1%), and tannic acid (1%) fixative with sucrose as an osmotic agent (Mercer *et al*., 1994). Fixed lung volume was measured by water displacement (Small, 1968). Coronal sections of lungs were embedded in paraffin and sectioned at a thickness of 5 μm with an HM 320 rotary microtome (Carl Zeiss, Thornwood, NY). Lung sections for histopathological evaluation were stained with hematoxylin and eosin or trichrome blue and examined by a board-certified veterinary pathologist for morphological alterations.

Lung Collagen Measurements

Total lung collagen content was determined using the Sircol Collagen Assay kit (Accurate Chemical and Scientific Corporation, Westbury, NY). Briefly, whole lungs were weighted and homogenized in 0.7 ml of 0.5M acetic acid–containing pepsin (Accurate Chemical and Scientific Corporation) with 1:10 ratio of pepsin: tissue wet weight. Each sample was stirred vigorously for 24 h at 4°C and centrifuged, and 200 μl of supernatant was assayed according to the manufacturer's instructions.

Statistics

Treatment-related differences in cytokine levels, cell counts, and collagen levels were evaluated using two-way ANOVA followed by pairwise comparison using the Student-Newman-Keuls tests, as appropriate. Statistical significance was considered at $p < 0.05$. Data are presented as mean ± SE.

Cytokine Analysis

Capture antibodies, biotinylated detection antibodies, and antigens for the sandwich ELISAs were purchased from R&D Systems (Minneapolis, MN) and stored as described previously (Gonzalez *et al*., 2008). ELISA microarray chips were manufactured in-house and processed as described previously (Gonzalez *et al*., 2008). Each of the capture antibodies was printed four times on each chip and once in each quadrant along with fluorescently labeled protein that served as an orientation marker. After printing, slides were blocked in 1% casein (Bio-Rad) and stored dry at −20°C until use. To generate standard curves, the antigen standards were combined into a single solution and serially diluted threefold in 0.1% casein to create seven concentrations of the standard mixture that spanned a 729-fold concentration range. A blank solution of 0.1% casein was also analyzed. Prior to analysis, BALF samples were diluted to 0.9×, 0.09×, and 0.009× of the original sample, such that the final solution contained 0.1% casein. Each dilution of each sample was analyzed in at least duplicate. The biotin signal from these antibodies was amplified using the biotinyltyramide amplification procedure followed by incubation with

streptavidin conjugated to a fluorescent dye (Varnum *et al*., 2004; Woodbury *et al*., 2002). Slides were washed with water and dried prior to fluorescent image analysis using a laser scanner (Perkin Elmer, Wellesley, MA). The spot intensity was quantified using software provided with the ScanArray Instrument. Standard curves were generated, and sample antigen concentrations were calculated using the Protein Microarray Analysis Tool (http://www.pnl.gov/statistics/ProMAT/; White *et al*., 2006).

Proteomics Work Flow

An overview of the work flow for the proteomics assessment is provided in Figure 1 and described in detail in the following sections.

Lung preparation for proteomics. Lung tissue was sonicated using an ultrasonic microprobe (Fisher Scientific, Houston, TX) on ice in 50% 2,2,2-trifluoroethanol and incubated 2 h at 37°C with gentle shaking. Protein concentration was determined using the bicinchoninic acid assay (Pierce, Rockford, IL). One hundred micrograms of protein from each sample was reduced with 2mM dithiothreitol, diluted fivefold with 50mM ammonium bicarbonate, pH 7.8, and digested with trypsin. Methylated, sequencing-grade trypsin (Promega, Madison, WI) was added at a substrate-to-enzyme ratio of 50:1 (mass:mass) and incubated at 37°C for 15 h. Sample cleanup was achieved using a solid phase extraction C_{18} column (Supelco, Bellefonte, PA) and the samples dried and stored at −20°C until analyzed by liquid chromatography mass spectroscopy (LC-MS).

LC-MS and data analysis. Lung tissue peptide samples were analyzed in duplicate using a custom-built automated pressure capillary LC system coupled to an 11.5-Tesla FTICR mass spectrometer (Harkewicz *et al*., 2002). The HPLC column was coupled to the mass spectrometer by an in-house–manufactured interface (Smith *et al*., 2002). The FTICR spectra were analyzed using the accurate mass and elution time (AMT) tag approach (Liu, 2007; Zimmer *et al*., 2006). Briefly, the theoretical mass and the observed normalized elution time (NET) of peptides identified by LC-MS/MS have been used previously to construct a reference database of murine mass and time (MT) tags (Pounds *et al*., 2008). Features from the LC-MS analyses (i.e., m/z peaks deconvolved of isotopic and charge state effects and then correlated by mass and NET) were matched to MT tags to identify peptides. The mass deisotoping and alignment process were performed using Decon2LS (Jaitly *et al*., 2009), and the matching process was performed using VIPER (Monroe *et al*., 2007) (http://ncrr.pnl.gov/software). Peptide data were further processed to remove peptides identified with low confidence using a uniqueness filter that required that the peptides have a spatial localized confidence score value of 0.5 or greater and a delta SLiC of 0.2 or greater (Monroe *et al*., 2007).

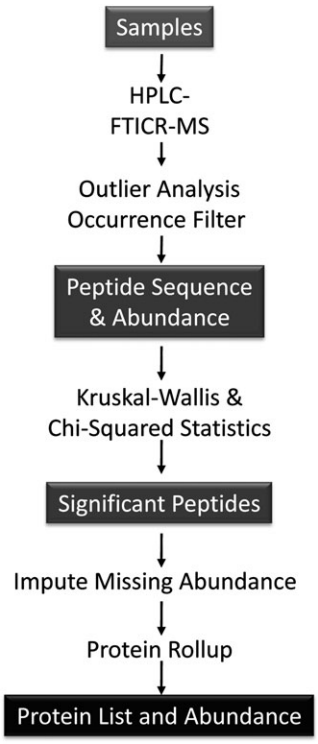

FIG. 1. Overview of work flow for proteomic analyses.

Peptides across duplicate runs of a biological sample are averaged ignoring missing values. Following this, the peptides are further occurrence filtered to those that have been observed in at least 50% of the samples from at least one treatment group. This filter accounts for the case where a peptide may be present for one of the treatment groups and not the other groups. This processing resulted in a set of 6032 peptides across the 26 samples.

Missing peptides are an experimental bias. To determine if this bias affects our data and corrects for it, all peptides observed fully, i.e., no missing values (1951 peptides), in the 26 biological samples were log transformed for normality and subjected to ANOVA. The within-sample summed peptide abundance should in theory be the same for all nonsignificant peptides. From the 1951 fully observed peptides, 1336 peptides had a p value > 0.1 and were collected as nonsignificant and correlated to the amount of missing data associated with each sample. The amount of missing data per sample ranged from 11.6 to 40.4% and were correlated ($R^2 = 0.82$) with the total abundance across the nonsignificant peptides. Thus, to correct for this bias, all observed values for each sample were divided by the average of the within-sample summed abundance of these 1336 for that sample.

Identification of significant peptides. The identification of statistically significant peptides was evaluated on the $\log_{10}$ normalized abundance. Because the missing data affect normality, a nonparametric version of ANOVA, Kruskal-Wallis, was used to assess significant differences between groups. Missing data can also be significant, e.g., when a peptide is completely missing from a treatment it may demonstrate the suppression of the expression of a specific protein. To address this issue, a modified chi-square test was used to determine if the amount of missing data in any group were less than expected by chance (Webb-Robertson *et al*., in preparation). The Kruskal-Wallis test identified 610 peptides with a significant differential abundance between at least two treatments (p value < 0.05). The chi-square test found that 105 peptides had a significant presence/absence pattern between at least two treatments (p value < 0.05). These two sets overlapped by seven peptides, yielding a total set of 708, or approximately 12% of the identified peptides, that were statistically significant.

Imputation strategy. Individual peptides may be absent from any given sample for two broad reasons. Either the peptide was not present in the biological sample or it is missing because of solely methodological problems such as fragmentation or identification problems. Imputation is a statistical approach to making determinations regarding the reason for the missing value and determining what abundance value if any should replace the "zero" value. We employ a "tiered" approach to imputation that uses the structure of the observed data to define the most appropriate imputation. In this case, if a peptide is completely missing from an individual treatment group, it is replaced with half of the minimum observed value for that peptide in other treatment groups. If a peptide is measured within a treatment group, any missing observations are replaced with the median of the observed values.

The median-based imputation strategy can introduce bias in the data that can lead to false identification of significance. We overcome this problem by performing the imputation on peptides that were identified as significant in the presence of the missing data, i.e., the 708 found significant with the Kruskal-Wallis and chi-square tests. Next, we evaluated if a peptide is significant when the rules of imputation are derived separately from data on that peptide. A bootstrapping algorithm was employed to derive an estimator of the p value associated with each peptide. Disjoint training and test sets were sampled 100 times, and the average p value and SE were computed. Large SEs suggest peptides that are only significant with specific separations of the data. Of the

708 significant peptides, 704 had a p value of less than 0.05 and 702 had a false discovery rate corrected q value of less than 0.05.

Partial least squares discriminant analysis. Partial least squares discriminant analysis (PLS-DA) was used to determine if the peptide abundance data could be used to discriminate between treatments. PLS-DA was run in MatLab Version R2008a using Version 4.2 of the PLS Toolbox from Eigenvector Research.

Protein rollup. The peptide abundance measurements were rolled up to the corresponding protein abundances using RRollup within DAnTE (http://ncrr.pnl.gov/software/; Polpitiya *et al*., 2008). Peptide redundancy—mapping to more than one protein—was reduced manually by selecting known proteins over similar but less completely annotated entries appearing as predicted proteins or hypothetical proteins.

Clustering by cellular process. Proteins were sorted and grouped by cellular process using their Gene Ontology (GO) annotations. GO process terms were matched to each protein using the Bioinformatics Resource Manager software (Shah *et al*., 2007), and protein expression patterns for each process group were clustered using the Multi-Experiment Viewer software (www.tm4.org/mev).

RESULTS

Histopathology and Biochemistry

There were no overt signs of toxicity or stress for the duration of the study and no reductions in weight or weight gain were observed.

As measured by the number of PMNs and the increase in total cell count of BALF, SWCNTs elicited a significantly greater inflammatory response compared with either crocidolite AB or UFCB (Fig. 2). Differences between crocidolite AB and UFCB were smaller and less consistent. AB caused statistically significant increases in total cells and PMNs, but not AM, whereas UFCB dosing leads to increases in all three cellular markers of the pulmonary inflammatory response. Despite repeated dosing and long pulmonary residence times, SWCNT treatments resulted in only modest increases in AM and crocidolite AB did not affect AM BALF. UFCB treatments led statistically significant elevations in total cell content, AM, and PMNs in BAL.

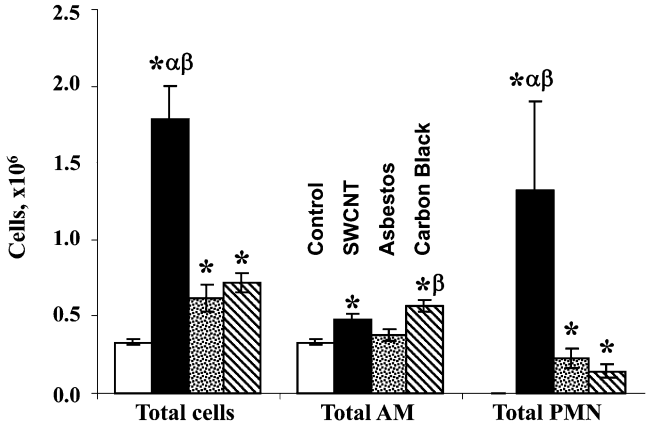

FIG. 2. Inflammatory cell content of BALF after repeated exposure of C57BL/6 mice to SWCNT, crocidolite AB, or UFCB (40 micrograms per mouse, twice a week, for 3 weeks). Open columns, PBS-exposed mice; black columns, SWCNT-exposed mice; dotted columns, AB-exposed mice; diagonal stripes columns, UFCB exposed mice. Mean + SEM ($n = 12$ mice per group). *, $p < 0.05$ versus control PBS-exposed mice; α, $p < 0.05$ vesrus AB-exposed mice; β, $p < 0.05$ versus UFCB exposed mice.

Lungs of SWCNT-exposed mice had the most profound inflammatory changes (Table 2, Fig. 3). Lungs from SWCNT-exposed mice had the most significant elevation in total BALF cells as well as PMNs. Moderate multifocal inflammation was present in all lungs from SWCNT-exposed mice (7/7) (Table 2, Fig. 2B). There was granuloma formation near bronchioles and adjacent alveoli consisting of round clusters of large macrophages and multinucleated giant cells that contained abundant greenish amorphous pigment. SWCNT agglomerates were observed within granulomas (Fig. 3). Many of these granulomas contained numerous polymorphonuclear cells (pyogranulomas), and some extended from the alveoli into the wall and lumen of the bronchiole. The granulomas circumscribed areas of fibrosis that extended for a short distance into surrounding septal walls. Pyogranulomas were observed in lungs from all SWCNT-exposed mice. Lungs from mice aspirated with AB had mild to moderate inflammation (Fig. 3, Table 2). The inflammation was characterized by alveoli, near bronchioles, containing large macrophages (histiocytes), many of which contained AB fibers of various lengths. Multinucleated giant cells were common, but classic granulomas were not observed. In some of these inflammatory foci, septal walls were thickened with mononuclear inflammatory cells. An occasional blood vessel had perivascular polymorphonuclear cells and mononuclear cells (chronic/active inflammation). An increase in fibrous tissue (minimal to mild) was observed in several specimens and was located in the larger foci of AM and when septal wall thickening was present. Collagen levels, a marker of fibrosis, were greatest in the SWCNT-treated mice (Fig. 4). AB and UFCB also caused statistically significant elevations in lung tissue collagen compared with control, but collagen deposition was significantly less than for SWCNTs (Fig. 4).

Lung sections from UFCB exposed mice had moderate histiocytosis (Fig. 3, Table 2) characterized by numerous histiocytes containing a small, cytoplasmic, black, and granular material. These histiocytes were diffusely distributed throughout the lung specimen, most often only one or two histiocytes in an alveolus. Near bronchioles, some alveoli had several histiocytes in an alveolus. There was very little inflammatory reaction in these lungs other than the histiocytosis. A few blood vessels had perivascular chronic active inflammation. Only one lung section was considered to have minimal fibrosis in the perivascular region (Fig. 3).

The pulmonary response following repeated p.a. of 40 μg of SWCNT was greater than for the same mass dose of crocidolite AB or UFCB for three endpoints: fibrosis (collagen deposition and histologically observed fibrosis), total cells, and PMNs in BALF. The incidence and severity of inflammatory and fibrotic

TABLE 2
Histopathology of Lungs from Mice after Repeated Aspiration of SWCNTs, AB, or UFCB

Method	Lesion	Process	Severity[a]	Distribution	PBS	UFCB	AB	SWCNT
H&E	Histiocytosis		Moderate	Diffuse		6/6		
	Inflammation		Minimal	Focal, subpleural	1/6			
	Inflammation		Mild	Perivascular		3/6		
	Inflammation	AM	Mild	Multifocal			2/6	
	Inflammation	AM	Moderate	Multifocal			4/6	
	Inflammation	Granuloma	Minimal	Focal		1/6		
	Inflammation	Pyogranulomatous	Moderate	Multifocal				7/7
TB	Histiocytosis		Moderate	Diffuse		5/6		
	Histiocytosis		Severe	Diffuse		1/6		
	Inflammation		Minimal	Focal, subpleural	1/6			
	Inflammation	AM	Mild	Multifocal			2/6	
	Inflammation	AM	Moderate	Multifocal			4/6	
	Inflammation	Pyogranulomatous	Moderate	Multifocal				7/7
	Fibrosis		Minimal			1/6	2/6	
	Fibrosis		Mild				4/6	7/7

Note. TB, trichrome blue; H&E, hemostatin and eosin.
[a]For all endpoints, the process appeared to be chronic rather than acute as was active for the perivascular inflammation in the UFCB group.

responses were greatest in mice treated with SWCNTs. All histopathological changes are summarized in Table 2.

Inflammatory Cytokine Levels in BALF

BALF levels of three cytokines, thymus and activation regulated chemokine (TARC), IL-12, and macrophage-derived cytokine (MDC), showed a pattern for the inflammatory response, SWCNTs > AB > UFCB, which is consistent with BAL PMN content, and histological markers of inflammation and fibrosis (Fig. 5). Matrix metalloproteinase-2 and macrophage inflammatory protein 1 gamma levels were increased in both the SWCNT and AB groups relative to control and UFCB treatments but did not differ significantly ($p < 0.05$, Kruskal–Wallis with a Bonferroni correction) between SWCNTs and AB. TARC is a cytokine

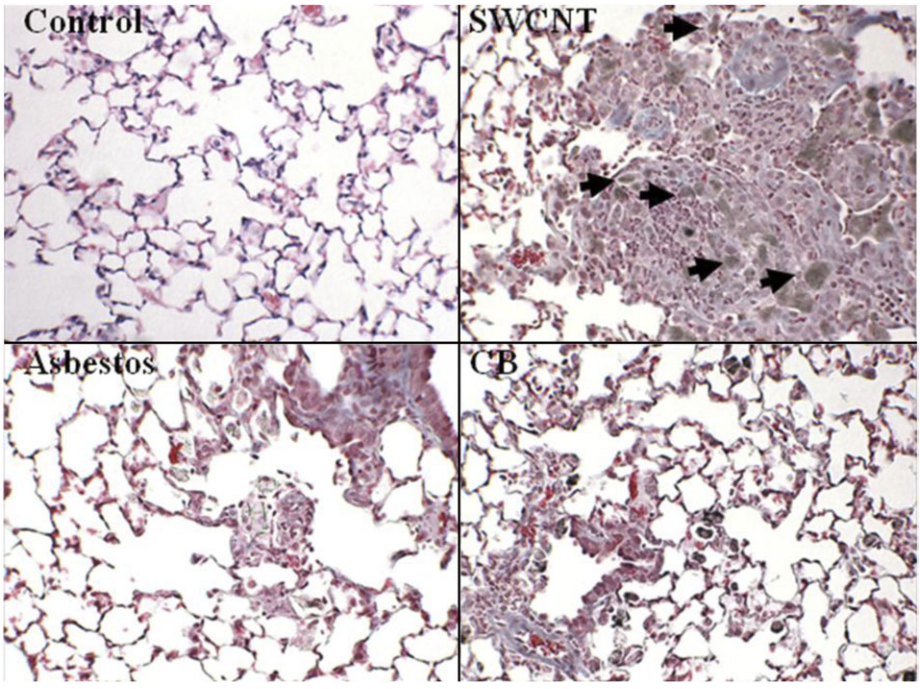

FIG. 3 Histopathology of lung from the SWCNT, AB, or UFCB repeated aspiration study (40 micrograms per mouse, twice a week, for 3 weeks): SWCNTs caused granuloma formation near bronchioles and adjacent alveoli. Fibrosis found within these granulomas extended for a short distance into surrounding septal walls. Arrows indicate agglomerates of SWCNTs within granulomas. In AB-treated animals, multinucleated giant cells were common, but classic granulomas were not observed, and an increase in fibrous tissue (minimal to mild) was observed in several specimens.

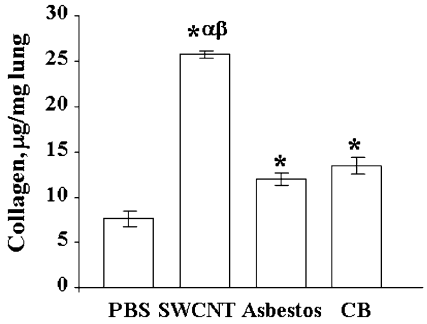

FIG. 4. Collagen accumulation in the lung of C57BL/6 mice after repeated aspiration of SWCNTs, AB, or UFCB (40 micrograms per mouse, twice a week, for 3 weeks). Mean + SEM ($n = 12$ mice per group). *, $p < 0.05$ versus control PBS-exposed mice; α, $p < 0.05$ versus AB-exposed mice; β, $p < 0.05$ versus UFCB exposed mice.

found in mononuclear cells that induce T-cell chemotaxis. MDC, is a T-cell chemotactic protein. IL-12 is an IL that induces TNF-α and modulates T-cell response to inflammation.

Protein Identification and Abundance

A total of 6032 unique peptides were identified across all lung tissue protein samples by matching their mass and elution time profiles to the AMT database following quality assurance and occurrence filtering (see Supplementary data S1). Rolling up the 6032 peptides produced a total of 5458 lung sample proteins. The number of peptides anchoring the protein identification ranged from 138 to 1, with approximately 50% of the proteins identified by a single peptide. Single peptide identifications are considered of sufficiently high confidence, given the use of 11-Tesla FTICR-MS and the AMT database for high accuracy identification of peptides and application of the occurrence filter, which eliminates low frequency (i.e., occurring by chance) peptides (and proteins). Kruskal-Wallis and chi-square tests identified 708 peptides whose abundance was affected by treatment by SWCNTs, AB, or UFCB. After imputation of missing abundance values, 702 peptides were identified as statistically significantly affected by treatment at the p value of 0.05. Rollup of these peptides produced a list of 408 proteins, of which 398 were statistically different from control (Dunnett's test, $p < 0.05$) (see Supplementary data S2).

SWCNT treatment affected the greatest number of proteins, 376, followed by AB (231) and UFCB (184). The trend in number of proteins affected followed the potency of these materials in four biochemical assays of inflammation (cytokines) and fibrosis as measured histologically but not by collagen deposition levels. The overall pattern of changes in protein abundance was remarkably similar across treatments, revealing broad similarities in the tissue-level response of the lung to the selected doses of SWCNTs, AB, and UFCB (Fig. 6). Ninety-six percent of the 231 proteins affected by AB treatment were also affected by SWCNT treatment (Fig. 7). Ninety-three percent and 69% of the 184 proteins whose abundance was affected by UFCB exposure were also affected

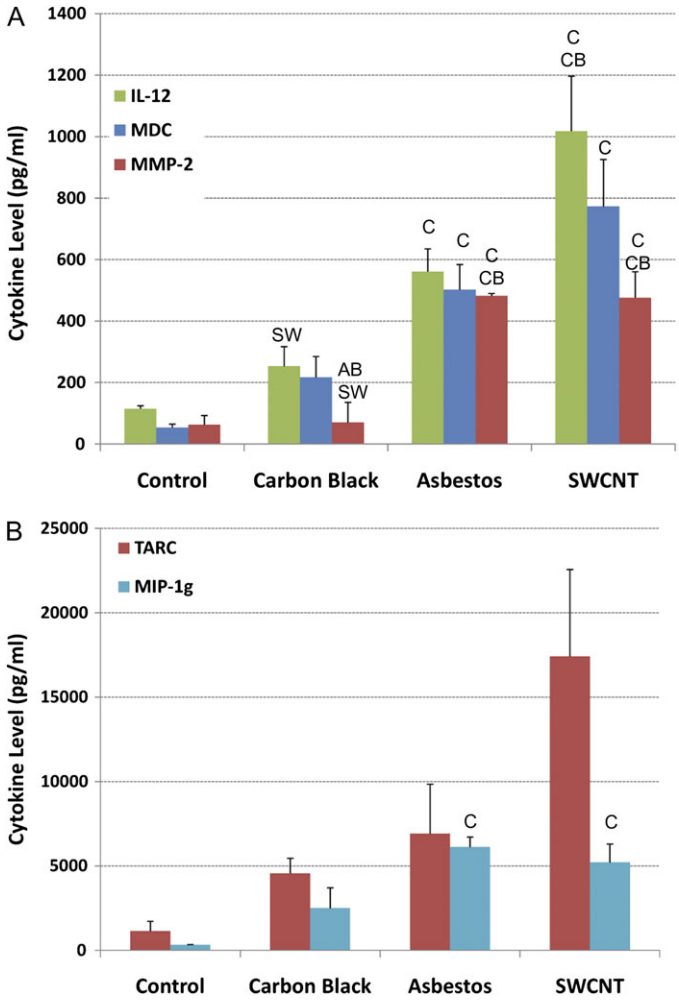

FIG. 5. Levels of the inflammatory cytokines IL-12, MDC, MMP-2 (panel A), and TARC and MIP-1g (panel B) in BALF measured by multiplexed MicroELISA. Three cytokines, TARC, IL-12, and MDC, show a pattern for the inflammatory response, SWCNTs > AB > UFCB, which is consistent with BAL PMN content and histological markers of inflammation and fibrosis. MMP-2 and MIP-1g levels were increased in both the SWCNT and AB groups relative to control and UFCB treatments but did not differ significantly between SWCNTs and AB. Data represent mean cytokine concentration per milliliter BAL ± SE with $n = 2$–8.

by SWCNTs or AB treatment, respectively. With few exceptions, the protein abundance data revealed an UFCB response, which was a subset of the AB response, which in turn was a subset of the SWCNT response (Fig. 7).

SWCNT treatment uniquely affected the abundance of 109 proteins (Supplementary data S3), whereas only a small number of proteins were unique to the AB (six) and carbon UFCB treatment groups (12).

Treatment Effects on Cellular Processes

To identify mechanistically important differences between treatments when at the level of cellular process rather than individual proteins, the 408 significant proteins were matched to GO cellular process terms and organized by functional

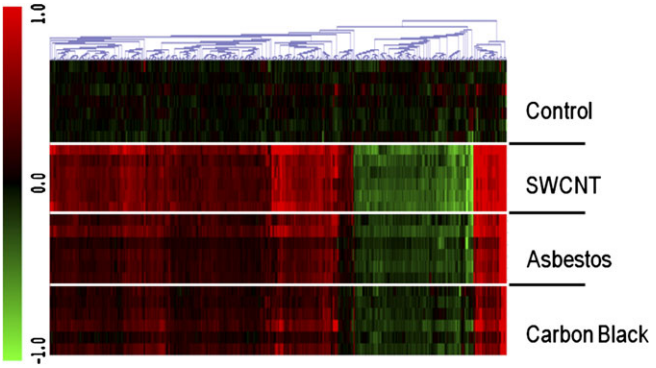

FIG. 6. Heat map of peptide abundance (ratio of log2 (abundance) to control), by treatment group, for the 708 of 5458 peptides affected by one or more treatments. The overall pattern of changes in peptide abundance is remarkably similar across treatments, revealing broad similarities in the pulmonary response of the lung to the selected doses of SWCNTs, AB, and UFCB after repeated administration. Black, unchanged compared with control; green, decreased abundance; and red, increased abundance compared with control.

categories of cellular processes. Seventy-two GO functional categories containing three or more GO terms each associated with a minimum of three significantly affected proteins were identified. The relative abundance of proteins in 13 GO functional categories related to inflammation/immune response, fibrosis, and tissue remodeling in response to SWCNTs, AB, and UFCB are presented as heat maps in Figure 8. The majority of the GO functional categories are associated with the immune response/inflammation: hematopoiesis, increases in chitinases, endocytosis, chemotaxis, immune response, leukocyte activation, and response to other organisms. Proteins involved in apoptosis and cell clearance/phagocytosis were also affected by exposure to UFCB, AB, and SWCNTs.

It is plausible that changes in proteins associated with secretion represent elaboration and expression of inflammatory cytokines. Epithelial cell morphogenesis and angiogenesis may be associated with adaptive or toxicity-driven tissue remodeling in response to the presence of the aspirated materials. Gene enrichment scores were calculated to evaluate the level of effect within the selected pathways. One of the 13 GO functional categories, chemotaxis, showed statistically significant

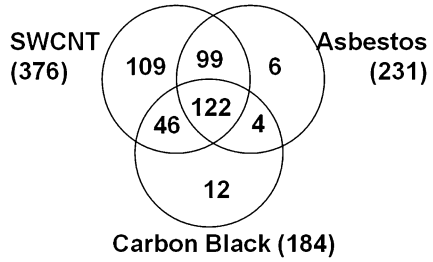

FIG. 7. Venn diagram showing the 398 proteins common or unique to SWCNT, AB, and UFCB treatment. Overall, a significantly smaller number of proteins were affected by AB and UFCB treatment than for SWCNT treatment. The list of proteins affected by AB and UFCB was almost entirely a subset of those affected by SWCNTs, implying a strong similarity in the pulmonary response to these materials measured by global proteomics.

enrichment, demonstrating the particularly strong response of chemotactic pathways.

We also tested whether the 109 proteins unique to SWCNT treatment represent effects on cellular processes not affected by either UFCB or AB. Categorizing the proteins by GO functional processes, we found that of the 22 functional processes associated with those 109 proteins whose abundance was only affected by SWCNT exposure, only six processes were unique to SWCNT exposure (Table 3). That is, the remaining 16 processes were also affected by AB treatment but were represented by different proteins.

Response Classification by PLS-DA

PLS-DA was used to determine if the peptide abundance data could be used to discriminate between treatments, i.e., whether some combination of affected proteins/peptides could represent a unique biosignature of response to each material. Despite the similarities in response across the materials, the PLS-DA clearly shows that the four groups (control, SWCNT, AB, and UFCB) are separable based on peptide information on the first three latent variables. A classification accuracy of 92.3%, or 24 of the 26, can be achieved with just the first three latent variables. The score plot (Fig. 9) shows that SWCNT mice are separated on the first component, control mice are separated on the second component (Fig. 9A), and AB and UFCB are separated on the third component (Fig. 9B) where the score of AB is largely negative and the opposite is observed for UFCB.

DISCUSSION

In response to wide recognition that SWCNTs bear toxicologically relevant similarities to asbestiform fibers and significant potential for human exposure, particularly in the occupational environment, multiple short-term CNT bioassays have been conducted in rodent models (Chou *et al.*, 2008; Lam *et al.*, 2004; Muller *et al.*, 2005, 2008; Shvedova *et al.*, 2005, 2007, 2008a, 2008c; Warheit *et al.*, 2004). The majority of the bioassays focused on selected, specific response of lung tissue to the presence of CNTs including inflammation, fibrosis, genetic toxicity, and a common sequence of events have emerged involving acute inflammation, formation of granulomas, and development of fibrosis. To some extent, these studies reflect a bias toward the expectation that the toxicologically important events will be consistent with other inflammogenic, fibrogentic materials such as AB. Consequently, it remains unknown whether, outside this focus, the tissue-level pulmonary response to SWCNTs is similar or dissimilar to AB. Broader, less focused assessments of the lung response to SWCNTs, for instance, by application of toxicogenomic approaches, have the advantage of assessing similarities and differences in response across thousands of response markers. We therefore sought to assess the similarities and differences between lung tissue responses to SWCNTs and crocidolite AB

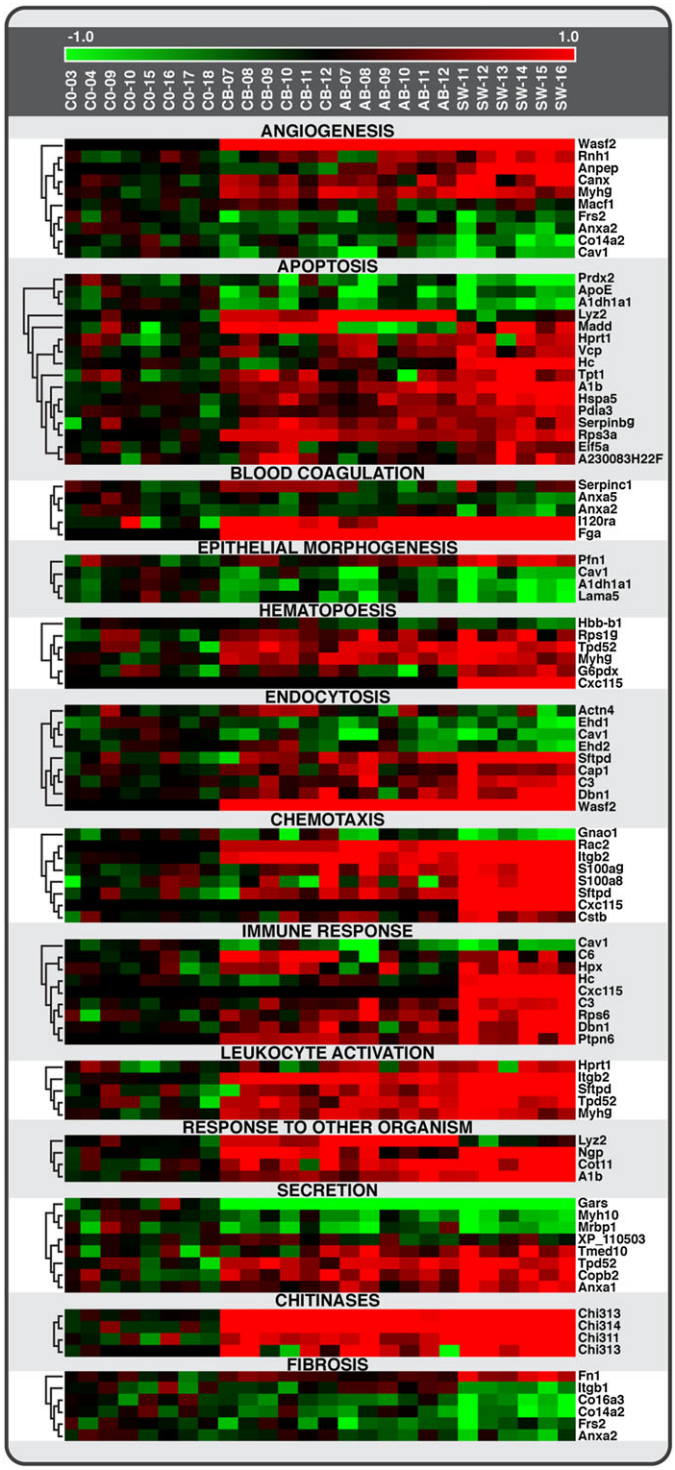

FIG. 8. Heat map showing protein levels for 13 cellular processes (GO functional categories) related to inflammation/immune response, fibrosis, and tissue remodeling in response to SWCNT, AB, and UFCB. Significant proteins were grouped according to nonredundant and biologically interpretable processes using their GO annotations. Consistent with the Venn diagrams, SWCNT appeared to have the strongest effect on protein levels for most biological processes. The abundance of S100a9 and Rps6 parallel the pattern of histopathological and biochemical markers of inflammation: SWCNT > AB > UFCB. S100a is a highly sensitive marker of inflammation also found in BALF of AB-exposed humans.

using high-sensitivity, HPLC-FTICR-MS–based proteomics. This study is the first global proteomic comparison lung response to SWCNTs and AB following exposure *in vivo*. Conventional histopathological and biochemical endpoints were also assessed to provide tissue-level context for the observed protein changes.

The lung inflammatory and fibrotic response, both incidence and severity, was greater for SWCNTs than for crocidolite AB or UFCB at the same mass dose as measured by collagen deposition, histologically observed fibrosis, and total cells and PMNs in BALF. The same relative inflammogenic potential, SWCNTs > AB > UFCB, was observed when assessed by the presence of three BAL cytokines, TARC, IL-12, and MDC. These three cytokines play important roles in control of the lung inflammatory response. TARC and MDC are structurally related T-cell chemokines expressed in macrophages. Both chemokines induce T-cell chemotaxis. IL-12–induced TNF-α also modulates T-cell response to inflammation. Thus, relative levels of these BAL cytokines parallel the level of histologically observed inflammation.

Measured by the number of treatment-affected proteins, a broad assessment of toxicological impact, SWCNTs (376 proteins) was also the most potent of the three tested materials (on a mass dose basis), followed by AB (231 proteins) and UFCB (184 proteins). Modest changes in lung tissue or lung BALF proteins have been reported in rodent models of diesel exhaust–induced inflammation (Lewis *et al.*, 2007) and in human models of endotoxin-induced pulmonary inflammation (de Torre *et al.*, 2006). Lewis *et al.* (2007) reported finding 20 treatment-related proteins by LC/MS in the BAL of male Sprague-Dawley rats exposed to diesel exhaust particles. Eleven of these proteins, Ager, Anxa1, Anxa5, s100a8, S100a9, Fga, Plunc, Prdx6, Sec14l3, and Sftpa1, were among those affected by treatment in our study. Chang *et al.* (2007) identified 33 proteins associated with lung injury/inflammation following intratracheal administration of 200 μg of carbon black in male ICR mice using 1-D gel electrophoresis coupled with LC/MS/MS analysis. The identified proteins provided evidence of damage to the lung epithelium, epithelial cell shedding, and oxidative stress. In a human model of endotoxin-induced pulmonary inflammation, de Torre *et al.* (2006) identified four BALF proteins associated with inflammation, S100a8, S100a9, ApoA1, and AT111 using 2-D gel electrophoresis and matrix-assisted laser desorption/ionization time of flight MS. The mouse homologue of the S1009a protein was also affected by treatment in our study, showing consistency between the human and mouse inflammatory response in the lung. Although there are a limited number proteomic-based studies to compare with, the much higher number of protein markers identified in our study may be the result of either the materials tested or the high sensitivity and effectiveness of the HPLC-FTICR-MS approach used in our study.

Differences in the pulmonary response to SWCNTs, AB, and UFCB in this study may be the result of significant

TABLE 3
GO Functional Categories Associated with the 109 Proteins Uniquely Affected by SWCNT Exposure

GO category	Proteins per category	Process unique to SWCNT?
Kidney development	3	Yes
Phosphorylation/metabolism	8	Yes
Carboxylic acid metabolism	3–4	Yes
Regulation of cell motility	3	Yes
Hemopoiesis	4	Yes
Cell redox homeostasis	4	Yes
Organ development	13–19	No
Organ morphogenesis	7–7	No
Cell morphogenesis	4–13	No
Angiogenesis	3–4	No
Tube morphogenesis	3–4	No
Myoblast/muscle development	4–5	No
Regulation of apoptosis	5–10	No
Monosaccharide/carbon metabolism	6–9	No
Translation	10–26	No
ATP/nucleotide metabolism	3–8	No
Anion transport	3–4	No
Protein metabolism	33–65	No
Neg regulation of biological process	10–14	No
Regulation of transcription	6–10	No
Intracellular transport	6–18	No
Endocytosis	4–6	No

differences in potency, differences in the time course of responses, or differences in doses. A single-dose, single-time-point study such as this one cannot provide a definitive answer to which of these give rise to the observations. This limitation is intrinsic and common to global toxicogenomic assessments of response because the costs of conducting such studies across time and dose are often very high. In addition, there is no accepted basis for comparing the dose of fibers (AB and SWCNTs) to nonfiber particulates because the latter lacks a major determinant of potency, namely, aspect ratio. In this study, the surface area doses of SWCNTs and UFCB were 125 or 30 times higher than the surface area dose of AB. Results should be interpreted accordingly, especially where evidence supports surface area–driven effects. For example, we report repeatedly that SWCNTs were generally more potent than AB, but if surface area alone determined the response to SWCNTs and AB, then AB, whose surface area–based dose was 125 less than for SWCNTs, would be the most potent material. Factoring in other aspects of these materials, transition metal content, and aspect ratio, we might come to yet another conclusion. Conclusions about relative toxicity based on mass doses can be valuable because exposure is often measured in these terms, but a study utilizing equivalent surface area doses of these compounds might be expected to conclude that SWCNTs are less potent than AB. Here we used well-characterized materials used in a larger body of literature on the pulmonary effects of SWCNTs and AB (Shvedova *et al.*, 2005) principally for broadly exploring the comparative biology of the response. Findings might not extrapolate to all SWCNT batches and types because of the diversity of physical and chemical properties of SWCNTs.

Despite differences in the potency of the materials as administered, there was broad similarity in the response to them. Global proteomic analysis revealed that 69 and 93% of proteins affected by AB and UFCB were also affected by SWCNT exposure, demonstrating that the AB and UFCB responses can be considered a subset of the proteins and biological processes affected by SWCNTs. These similarities held when affected proteins were organized by biological processes using GO functional categories. Overall, there was evidence of a strong inflammatory response (hematopoiesis, immune response,

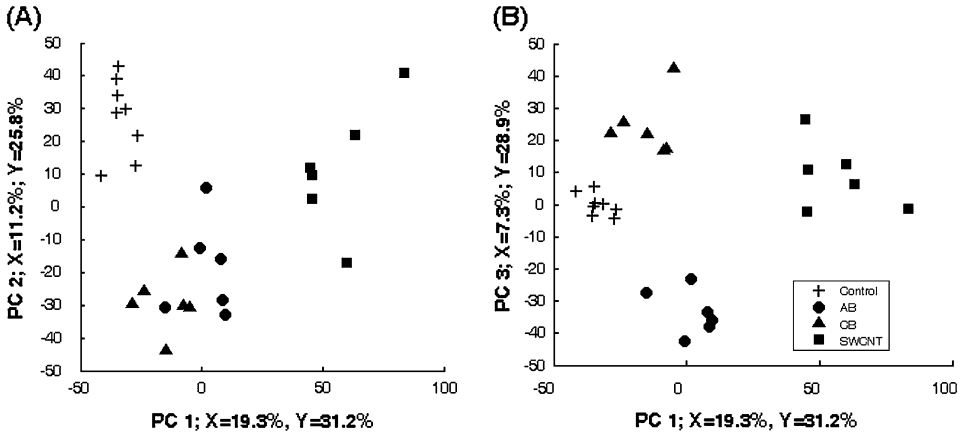

FIG. 9. Scores plot from PLS-DA of 708 significant peptides. PLS-DA was used to determine if the peptide abundance data could be used to discriminate between treatments. SWCNT are separated on the first component, controls are separated on the second component (panel A), and AB and UFCB are separated on the third component (panel B). The PLS analysis indicates that the peptide data accurately distinguish between treatments, suggesting the presence of a unique biosignature for each material in the peptide data.

leukocyte activation, and secretion), fibrosis, tissue remodeling (epithelial morphogenesis and angiogenesis), cytotoxicity (apoptosis), and response to the presence of foreign materials (response to other organism, chitinases, endocytosis). Parallel similarities were observed in lung tissue: inflammatory effects (histiocytosis and inflammation) generally increasing in incidence/severity in the order UFCB < AB < SWCNTs, more chronic inflammation (pyrogranulomatous and SWCNTs only), and finally the fibrosis, the product of chronic unresolved inflammation, also with increasing incidence in the order UFCB < AB < SWCNT.

The cellular processes affected by *in vivo* SWCNT exposure were similar to those affected by *in vitro* exposure of human monoblastic leukemia cells to 10 mg/ml MWCNT. (Haniu *et al*., 2010). Haniu *et al*. (2010) reported altered abundance of 37 proteins comprising 17 GO functional categories. The majority of the cellular processes were nonspecific, including general metabolism (lipid and protein metabolic processes, catalytic process, biosynthetic process, and carbohydrate metabolic process), regulation (transcription and translation), cell cycle (cell death, cell proliferation, cell differentiation, and multicellular organismal development), and signaling (signal transduction/cell communication). With the exception of lipid metabolic process and response to stress, all these cellular processes were also observed to be affected by SWCNT treatment *in vivo* in our study. The absence of immune- and inflammation-related processes in the *in vitro* data highlights the importance of using dose-route relevant cells for *in vitro* systems, e.g., macrophages or bronchiolar epithelial cells, as well as for using whole animals representing the integrated function of the system in assessing response to nanomaterials.

The abundance of S100a9, a highly sensitive marker of inflammation found in BALF of AB-exposed workers (Archimandriti *et al*., 2009), paralleled the pattern of histopathological and biochemical markers of inflammation: SWCN > AB > UFCB. S100 proteins are calcium-binding proteins overexpressed on the membrane surface of phagocytes at sites of inflammation. This report is the first to show that S100a9 expression is affected by AB in a rodent model of lung inflammation; given S100a9's close correlation to the level of inflammation, this protein may be an excellent biomarker of inflammatory response to SWCNTs or other inflammogenetic materials in exposed workers. CxCL15, a chemotactic cytokine, was uniquely increased in the SWCNT group, raising the possibility that this cytokine could be used as a marker of SWCNT exposure.

The abundance of the chitinase-like proteins CHI3L1, CHI3L3, and CHI3L4 were consistently higher following exposure to UFCB, AB, and SWCNTs relative to control lung samples, showing no significant material-related differences. CHI3L1 (Ym1) is a secreted glycoprotein found at low nanomolar levels in plasma and some tissues (Coffman, 2008). Its expression levels, and blood levels, have been correlated with chronic inflammatory conditions and related diseases (Coffman, 2008). Macrophages and neutrophils are secretory sources of CHI3L1 in the lung where the protein likely acts as either a mitogen or a chemotactic factor (Coffman, 2008) involved in the inflammatory response. CHI3L3 interacts directly with type I collagen and may also play a role in tissue remodeling, proteomic evidence of which was observed after exposure to AB, UFCB, and SWCNTs. CHI3L3 (Ym1) messenger RNA is elevated in lung tissue of mice exposed to diesel exhaust particles and is hypothesized to play a role in airway inflammation and responsiveness (Song *et al*., 2008). CHI3L3 and the related protein, CHI3L4 (Ym2), are both associated with the asthmatic lung and by virtue of sequence homology to proteins involved in tissue remodeling are hypothesized to play a role in tissue remodeling during allergic responses (Webb *et al*., 2001).

Several treatment-modulated proteins involved in chemotaxis are expressed specifically in phagocytes or PMNs rather than lung epithelial cells. S1009a, a proinflammatory marker also reported to have the capacity to scavenge oxidants, is abundantly expressed in PMNs and neutrophils (Goyette and Geczy, 2010; Lim *et al*., 2009). Ras-related C3 botulinum toxin substrate 2 (RAC2) is solely expressed in hematopoietic cells (Hordijk, 2006) such as PMNs. RAC2 is a key regulator of chemotaxis required for macrophage accumulation during peritoneal inflammation. In addition, RAC2 regulates NAPDH oxidase activity in neutrophils, which is a central component of the phagosome pathogen killing apparatus (Diebold and Bokoch, 2005). B-integrin is a leukocyte-specific regulator of cell adhesion, transendothelial migration, and phagocytosis expressed in PMNs (Mayadas and Cullere, 2005; Schymeinsky *et al*., 2007). Other proteins were associated with the lung epithelium. Lungkine (CXXL15), a chemokine expressed in mouse lung airway epithelial cells that induces neutrophil recruitment (Chen *et al*., 2001), was significantly increased after SWCNT treatment, as was surfactant D (Sftpd), an opsin and modulator of macrophage phagocytosis (Pastva *et al*., 2007). The identification of these proteins in the lung tissue is evidence that the proteomic approach applied here is capable of revealing responses not only in lung tissue, e.g., increased expression of PMN chemokines (e.g., Lunkine), but also effects associated with PMN influx (e.g., RAC2 and S100a9).

The finding that there were sufficient differences in the response to these materials at the level of peptides to classify the materials based on responses with high accuracy does not contradict our finding of broad similarities in the response based on mechanistic interpretations of the histopathological, biochemical, and proteomic data. The PLS analysis identified patterns in the abundance of three groups (components) of peptides from a set of 708 affected peptides that could be used to distinguish between the materials but did not establish that the peptide components represent biologically important difference related to the observed pathology.

Surprisingly, we found that the 109 proteins uniquely affected by SWCNTs, which could be interpreted as evidence of a significant difference in biological response compared with

the other materials, were associated with unique cellular processes in only a few cases. Most of the cellular processes represented by these 109 proteins were also represented in the AB group by other proteins. Six processes, phosphorylation/metabolism, carboxylic acid metabolism, regulation of cell motility, hematopoiesis, cell redox homeostasis, and kidney development, were exceptions, though the mechanistic interpretation and implication of these cellular processes is difficult. The involvement of cell redox homeostasis in the SWCNT response suggests a high level of oxidative stress, either directly from the SWCNTs or indirectly from the resulting inflammation.

Overall, the proteomic analysis is supportive of the broad conclusion that lung tissue and lung infiltrate responses to SWCNTs and crocidolite AB were similar, but like several histopathological endpoints, the response was generally greater on a mass dose basis for SWCNTs than for either AB or UFCB.

SUPPLEMENTARY DATA

Supplementary data are available online at http://toxsci.oxfordjournals.org/.

FUNDING

This research was collaboration between the Pacific Northwest National Laboratory and the National Institute of Occupational Safety and Health. Portions of this work were funded by the U.S. Department of Energy through the Environmental Biomarkers Initiative at Pacific Northwest National Laboratory (PNNL). Some of the experimental work was performed in the Environmental Molecular Sciences Laboratory, a U.S. Department of Energy, Office of Biological and Environmental Research national scientific user facility on the PNNL campus. PNNL is multi-program national laboratory operated by Battelle for the DOE under Contract No. DE-AC05-76RLO 1830. Also supported by NIOSH (Grant No. OH008282), National Occupational Research Agenda (NORA) (Grant No. 927ZJHF), National Institutes of Health (NIH), and the 7th Framework Programme of the European Commission (EC-FP7- NANOMUNE).

REFERENCES

Archimandriti, D. T., Dalavanga, Y. A., Cianti, R., Bianchi, L., Manda-Stachouli, C., Armini, A., Koukkou, A. I., Rottoli, P., Constantopoulos, S. H., and Bini, L. (2009). Proteome analysis of bronchoalveolar lavage in individuals from Metsovo, nonoccupationally exposed to asbestos. *J. Proteome Res.* **8,** 860–869.

Baughman, R. H., Zakhidov, A. A., and d. Heer, W. A. (2002). Carbon nanotubes—the route toward applications. *Sci. Technol. Lett.* **297,** 787–792.

Chang, C. C., Chen, S. H., Ho, S. H., Yang, C. Y., Wang, H. D., and Tsai, M. L. (2007). Proteomic analysis of proteins from bronchoalveolar lavage fluid reveals the action mechanism of ultrafine carbon black-induced lung injury in mice. *Proteomics* **7,** 4388–4397.

Chen, S. C., Mehrad, B., Deng, J. C., Vassileva, G., Manfra, D. J., Cook, D. N., Wiekowski, M. T., Zlotnik, A., Standiford, T. J., and Lira, S. A. (2001). Impaired pulmonary host defense in mice lacking expression of the CXC chemokine lungkine. *J. Immunol.* **166,** 3362–3368.

Chou, C. C., Hsiao, H. Y., Hong, Q. S., Chen, C. H., Peng, Y. W., Chen, H. W., and Yang, P. C. (2008). Single-walled carbon nanotubes can induce pulmonary injury in mouse model. *Nano Lett.* **8,** 437–445.

Coffman, F. D. (2008). Chitinase 3-Like-1 (CHI3L1): a putative disease marker at the interface of proteomics and glycomics. *Crit. Rev. Clin. Lab. Sci.* **45,** 531–562.

de Torre, C., Ying, S. X., Munson, P. J., Meduri, G. U., and Suffredini, A. F. (2006). Proteomic analysis of inflammatory biomarkers in bronchoalveolar lavage. *Proteomics* **6,** 3949–3957.

Diebold, B. A., and Bokoch, G. M. (2005). Rho GTPases and the control of the oxidative burst in polymorphonuclear leukocytes. *Curr. Top. Microbiol. Immunol.* **291,** 91–111.

Donaldson, K., Stone, V., Seaton, A., Tran, L., Aitken, R., and Poland, C. (2008). Re: induction of mesothelioma in p53+/- mouse by intraperitoneal application of multi-wall carbon nanotube. *J. Toxicol. Sci.* **33,** 385 author reply 386–388.

Gonzalez, R. M., Seurynck-Servoss, S. L., Crowley, S. A., Brown, M., Omenn, G. S., Hayes, D. F., and Zangar, R. C. (2008). Development and validation of sandwich ELISA microarrays with minimal assay interference. *J. Proteome Res.* **7,** 2406–2414.

Goyette, J., and Geczy, C. L. (2010). Inflammation-associated S100 proteins: new mechanisms that regulate function. *Amino Acids.* Advance Access published on May 6, 2010; doi: 10.1007/s00726-010-0528-0.

Haniu, H., Matsuda, Y., Takeuchi, K., Kim, Y. A., Hayashi, T., and End, M. (2010). Proteomics-based safety evaluation of multi-walled carbon nanotubes. *Toxicol. Appl. Pharmacol.* **242,** 256–262.

Harkewicz, R., Belov, M. E., Anderson, G. A., Pasa-Tolic, L., Masselon, C. D., Prior, D. C., Udseth, H. R., and Smith, R. D. (2002). ESI-FTICR mass spectrometry employing data-dependent external ion selection and accumulation. *J. Am. Soc. Mass Spectrom.* **13,** 144–154.

Hordijk, P. L. (2006). Regulation of NADPH oxidases: the role of Rac proteins. *Circ. Res.* **98,** 453–462.

Ijima, S. (1991). Helical microtubules of graphite carbon. *Nature* **354,** 56–58.

Jaitly, N., Mayampurath, A., Littlefield, K., Adkins, J. N., Anderson, G. A., and Smith, R. D. (2009). Decon2LS: an open-source software package for automated processing and visualization of high-resolution mass spectrometry data. *BMC Bioinformatics* **10,** 87.

Kisin, E., Murray, A. R., Schwegler-Berry, D., Scabilloni, J., Mercer, R. R., Chirila, M., Young, S., Leonard, S., Keohavong, P., Fadeel, B., *et al.* Pulmonary response, oxidative stress and genotoxicity induced by carbon nanofibers. *Toxicologist,* **2010,** 169.

Lam, C. W., James, J. T., McCluskey, R., and Hunter, R. L. (2004). Pulmonary toxicity of single-wall carbon nanotubes in mice 7 and 90 days after intratracheal instillation. *Toxicol. Sci.* **77,** 126–134.

Lewis, J. A., Rao, K. M., Castranova, V., Vallyathan, V., Dennis, W. E., and Knechtges, P. L. (2007). Proteomic analysis of bronchoalveolar lavage fluid: effect of acute exposure to diesel exhaust particles in rats. *Environ. Health Perspect.* **115,** 756–763.

Lim, S. Y., Raftery, M. J., Goyette, J., Hsu, K., and Geczy, C. L. (2009). Oxidative modifications of S100 proteins: functional regulation by redox. *J. Leukoc. Biol.* **86,** 577–587.

Liu, T., Belov, M. E., *et al.* (2007). Accurate mass measurements in proteomics. *Chem. Rev.* **107,** 3621–3653.

Ma-Hock, L., Treumann, S., Strauss, V., Brill, S., Luizi, F., Mertler, M., Wiench, K., Gamer, A. O., van Ravenzwaay, B., and Landsiedel, R. (2009).

Inhalation toxicity of multiwall carbon nanotubes in rats exposed for 3 months. *Toxicol. Sci.* **112,** 468–481.

Mayadas, T. N., and Cullere, X. (2005). Neutrophil beta2 integrins: moderators of life or death decisions. *Trends Immunol.* **26,** 388–395.

Maynard, A. D., Baron, P. A., Foley, M., Shvedova, A. A., Kisin, E. R., and Castranova, V. (2004). Exposure to carbon nanotube material: aerosol release during the handling of unrefined single-walled carbon nanotube material. *J. Toxicol. Environ. Health A* **67,** 87–107.

Mercer, R. R., Russell, M. L., and Crapo, J. D. (1994). Alveolar septal structure in different species. *J. Appl. Physiol.* **77,** 1060–1066.

Monroe, M. E., Tolic, N., Jaitly, N., Shaw, J. L., Adkins, J. N., and Smith, R. D. (2007). VIPER: an advanced software package to support high-throughput LC-MS peptide identification. *Bioinformatics* **23,** 2021–2023.

Muller, J., Huaux, F., Fonseca, A., Nagy, J. B., Moreau, N., Delos, M., Raymundo-Piñero, E., Béguin, F., Kirsch-Volders, M., and Fenoglio, I. (2008). Structural defects play a major role in the acute lung toxicity of multiwall carbon nanotubes: toxicological aspects. *Chem. Res. Toxicol* **21,** 1698–1705.

Muller, J., Huaux, F., Moreau, N., Misson, P., Heilier, J. F., Delos, M., Arras, M., Fonseca, A., Nagy, J. B., Lison, D., *et al.* (2005). Respiratory toxicity of multi-wall carbon nanotubes. *Toxicol. Appl. Pharmacol.* **207,** 221–231.

Pacurari, M., Castranova, V., and Vallyathan, V. (2010). Single- and multi-wall carbon nanotubes versus asbestos: are the carbon nanotubes a new health risk to humans? *J. Toxicol. Environ. Health A* **73,** 378–395.

Pastva, A. M., Wright, J. R., and Williams, K. L. (2007). Immunomodulatory roles of surfactant proteins A and D: implications in lung disease. *Proc. Am. Thorac. Soc.* **4,** 252–257.

Pauluhn, J. (2010). Subchronic 13-week inhalation exposure of rats to multiwalled carbon nanotubes: toxic effects are determined by density of agglomerate structures, not fibrillar structures. *Toxicol. Sci.* **113,** 226–242.

Polpitiya, A. D., Qian, W. J., Jaitly, N., Petyuk, V. A., Adkins, J. N., Camp, D. G. 2nd, Anderson, G. A., and Smith, R. D. (2008). DAnTE: a statistical tool for quantitative analysis of -omics data. *Bioinformatics* **24,** 1556–1558.

Pounds, J. G., Flora, J. W., Adkins, J. N., Lee, K. M., Rana, G. S., Sengupta, T., Smith, R. D., and McKinney, W. J. (2008). Characterization of the mouse bronchoalveolar lavage proteome by micro-capillary LC-FTICR mass spectrometry. *J. Chromatogr. B Analyt. Technol. Biomed. Life Sci.* **864,** 95–101.

Rao, G., Tinkle, S., Weissman, D. N., Antonini, J. M., Kashon, M. L., Salmen, R., Battelli, L. A., Willard, P. A., Hoover, M. D., and Hubbs, A. F. (2003). Efficacy of a technique for exposing the mouse lung to particles aspirated from the pharynx. *J. Toxicol. Environ. Health* **66,** 1441–1452.

Sanchez, V. C., Pietruska, J. R., Miselis, N. R., Hurt, R. H., and Kane, A. B. (2009). Biopersistence and potential adverse health impacts of fibrous nanomaterials: what have we learned from asbestos? *Wiley Interdiscip. Rev. Nanomed. Nanobiotechnol.* **1,** 511–529.

Schymeinsky, J., Mocsai, A., and Walzog, B. (2007). Neutrophil activation via beta2 integrins (CD11/CD18): molecular mechanisms and clinical implications. *Thromb. Haemost.* **98,** 262–273.

Shah, A. R., Singhal, M., Klicker, K. R., Stephan, E. G., Wiley, H. S., and Waters, K. M. (2007). Enabling high-throughput data management for systems biology: the bioinformatics resource manager. *Bioinformatics* **23,** 906–909.

Shvedova, A. A., Fabisiak, J. P., Kisin, E. R., Murray, A. R., Roberts, J. R., Tyurina, Y. Y., Antonini, J. M., Feng, W. H., Kommineni, C., Reynolds, J., *et al.* (2008a). Sequential exposure to carbon nanotubes and bacteria enhances pulmonary inflammation and infectivity. *Am. J. Respir. Cell Mol. Biol.* **38,** 579–590.

Shvedova, A. A., Kisin, E., Murray, A. R., Johnson, V. J., Gorelik, O., Arepalli, S., Hubbs, A. F., Mercer, R. R., Keohavong, P., Sussman, N., *et al.* (2008b). Inhalation vs. aspiration of single-walled carbon nanotubes in C57BL/6 mice: inflammation, fibrosis, oxidative stress, and mutagenesis. *Am. J. Physiol. Lung Cell Mol. Physiol.* **295,** L552–L565.

Shvedova, A. A., Kisin, E. R., Mercer, R., Murray, A. R., Johnson, V. J., Potapovich, A. I., Tyurina, Y. Y., Gorelik, O., Arepalli, S., Schwegler-Berry, D., *et al.* (2005). Unusual inflammatory and fibrogenic pulmonary responses to single-walled carbon nanotubes in mice. *Am. J. Physiol. Lung Cell Mol. Physiol.* **289,** L698–L708.

Shvedova, A. A., Kisin, E. R., Murray, A. R., Gorelik, O., Arepalli, S., Castranova, V., Young, S. H., Gao, F., Tyurina, Y. Y., Oury, T. D., *et al.* (2007). Vitamin E deficiency enhances pulmonary inflammatory response and oxidative stress induced by single-walled carbon nanotubes in C57BL/6 mice. *Toxicol. Appl. Pharmacol.* **221,** 339–348.

Shvedova, A. A., Kisin, E. R., Murray, A. R., Kommineni, C., Castranova, V., Fadeel, B., and Kagan, V. E. (2008c). Increased accumulation of neutrophils and decreased fibrosis in the lung of NADPH oxidase-deficient C57BL/6 mice exposed to carbon nanotubes. *Toxicol. Appl. Pharmacol.* **231,** 235–240.

Small, J. (1968). Measurements of section thickness. In *Proceedings 4th European Congress on Electron Microscopy* (D. S. Bociarelli, Ed.), Vol. 1, pp. 609–610. Tipografia Poliglotta Vaticana, Rome, Italy.

Smith, R. D., Anderson, G. A., Lipton, M. S., Pasa-Tolic, L., Shen, Y., Conrads, T. P., Veenstra, T. D., and Udseth, H. R. (2002). An accurate mass tag strategy for quantitative and high-throughput proteome measurements. *Proteomics* **2,** 513–523.

Song, H. M., Jang, A. S., Ahn, M. H., Takizawa, H., Lee, S. H., Kwon, J. H., Lee, Y. M., Rhim, T. Y., and Park, C. S. (2008). Ym1 and Ym2 expression in a mouse model exposed to diesel exhaust particles. *Environ. Toxicol.* **23,** 110–116.

Thayer, A. M. (2007). Carbon nanotubes by the metric ton anticipating new commercial applications, producers increase capacity. *Chem. Eng. News* **85,** 29–35.

Varnum, S. M., Woodbury, R. L., and Zangar, R. C. (2004). A protein microarray ELISA for screening biological fluids. *Methods Mol. Biol.* **264,** 161–172.

Warheit, D. B., Laurence, B. R., Reed, K. L., Roach, D. H., Reynolds, G. A., and Webb, T. R. (2004). Comparative pulmonary toxicity assessment of single-wall carbon nanotubes in rats. *Toxicol. Sci.* **77,** 117–125.

Webb, D. C., McKenzie, A. N., and Foster, P. S. (2001). Expression of the Ym2 lectin-binding protein is dependent on interleukin (IL)-4 and IL-13 signal transduction: identification of a novel allergy-associated protein. *J. Biol. Chem.* **276,** 41969–41976.

Webb-Robertson, B. J. M., McCue, L. A., Waters, K. M., Matzke, M. M., Jacobs, J. M., Metz, T. O., Varnum, S., and Pounds, J. G. (2010). Combined statistical analyses of peptide intensities and peptide occurrences improves identification of significant peptides from MS-based proteomics data. *J Proteome Res.* **9,** 5748–5756.

White, A. M., Daly, D. S., Varnum, S. M., Anderson, K. K., Bollinger, N., and Zangar, R. C. (2006). ProMAT: protein microarray analysis tool. *Bioinformatics* **22,** 1278–1279.

Witasp, A., Nordfors, L., Schalling, M., Nygren, J., Ljungqvist, O., and Thorell, A. (2009). Increased expression of inflammatory pathway genes in skeletal muscle during surgery. *Clin. Nutr.* **28,** 291–298.

Woodbury, R. L., Varnum, S. M., and Zangar, R. C. (2002). Elevated HGF levels in sera from breast cancer patients detected using a protein microarray ELISA. *J. Proteome Res.* **1,** 233–237.

Zimmer, J. S., Monroe, M. E., Qian, W. J., and Smith, R. D. (2006). Advances in proteomics data analysis and display using an accurate mass and time tag approach. *Mass Spectrom Rev* **25,** 450–482.